NUEJ
Naresuan University
Engineering Journal

Enhancing Flood Susceptibility Mapping using Statistical and Machine Learning Approaches: A Case Study of the Wang River Basin, Thailand

Gen Long[1], Sarintip Tantanee[2,*], Korakod Nusit[3] and Pitikhate Sooraksa[4]

[1,3] Civil of Engineering Department, Faculty of Engineering, Naresuan University, Phitsanulok 65000, Thailand
[2] Center of Excellence on Energy Technology and Environment, Faculty of Engineering, Naresuan University, Phitsanulok 65000, Thailand
[4] Department of Robotics and AI, School of Engineering, King Mongkut's Institute of Technology, Ladkrabang, 1 Chalongkrung 1, Ladkrabang, Bangkok 10520, Thailand

* Corresponding author e-mail: sarintipt@nu.ac.th

(Received: 2 February 2025, Revised: 20 April 2025, Accepted: 20 April 2025)

Abstract

In flood-vulnerable regions like the Wang River Basin, Thailand, flood susceptibility mapping (FSM) plays a key role in flood disaster risk management. However, the comparative performance between traditional statistical methods and machine learning (ML) algorithms for FSM under identical conditions has not been thoroughly explored. This research investigates the performance of Shannon's Entropy (SE), a statistical model, and Random Forest (RF), a ML algorithm for the prediction of flood-potential areas. Multicollinearity analysis together with SE-based weighting identified a total of seven significant flood conditioning factors (FCFs) which are curvature, slope, elevation, geology, soil permeability, precipitation, and stream power index (SPI). The models were trained and validated using 3,000 flood and 3,000 non-flood points with a ratio of 70:30. Results showed that the RF model outperformed SE with AUC-ROC values of 0.929 (training) and 0.931 (verification), compared to SE of which are 0.874 and 0.870, indicating the superiority of ML in handling complex environmental data, which can offer advantages in flood risk prediction. This study also presents the promise of ML in enhancing FSM accuracy and confidence, enabling risk mitigation strategies in the Wang River Basin and similar areas.

Keywords: Flood susceptibility mapping, Machine learning (ML), Random Forest (RF), Shannon's Entropy (SE), Wang River Basin.

1. INTRODUCTION

Floods are one of the most severe natural disasters worldwide, responsible for massive socio-economic losses and environmental losses (Bhattarai et al., 2024). The Wang River Basin in Thailand, a critical tributary of the Chao Phraya River, is subject to frequent flooding driven by climatic and anthropogenic change (Charoenlerkthawin et al., 2021). Extreme events like 2011 floods highlighted an immediate need to develop reliable flood sustainability modelling to undertake mitigating measures. The use of common statistical methods such as SE for FSM remained prevalent due to their relative straightforwardness and interpretability (Haghizadeh et al., 2017). On the other hand, improvements in ML algorithms, especially RF, proved to be superior in their ability to be able to represent non-linearity in complex geospatial data sets (Kaya & Derin, 2023; Seydi et al., 2022).

Numerous recent studies emphasized the superiority of ML-based methods for FSM. For instance, Tehrany et al. (2019) demonstrated that ML models outperform conventional approaches in identifying flood-prone areas by leveraging multi-dimensional environmental variables. Similarly, Bhattarai et al. (2024) highlighted that RF was an efficient tool in assessment of transboundary river basins with its fast, reliable and efficient capacity. Dey et al. (2024) compared different decision tree-based ML models such RF, Adaptive Boosting (AdaBoost), Gradient Boosting (GdBoost), and Extreme Gradient Boosting (XGBoost) against a classical Frequency Ratio (FR) model. The study results showed all the ML models performed better than the FR model, with the RF model producing an area under the curve (AUC) of 0.85. Furthermore, Wahba et al. (2024) investigated the efficacy of various ML approaches in generating FSMs, finding that artificial neural networks (ANN-MLP) and support vector regression (SVR) were highly accurate, giving AUC values of 95.23% and 95.83%, respectively. Nevertheless, challenges persist for ML, including limited data availability, model interpretability, and regional applicability (Wahba et al., 2024).

To fill these gaps, this study compared SE and RF models in the context of the Wang River Basin. Seven FCFs—validated through multicollinearity checks and SE-based FCF selection and weighting—were adopted to generate high-resolution susceptibility maps. The objectives were threefold: (1) to identify critical FCFs driving flood susceptibility in the study area, (2) to evaluate the predictive accuracy of SE and RF models, and (3) to provide spatially explicit insights for flood risk management. By leveraging recent methodological

innovations and empirical validations, this work contributed to the growing body of literature on ML-driven FSM, offering scalable solutions for flood-prone regions.

2. STUDY AREA

The Wang River Basin (Figure 1), located in northern Thailand, is the smallest sub-basin of the Upper Chao Phraya River system, covering approximately 10,800 km². The basin lies between 17°05′N–19°30′N latitude and 98°54′E–99°58′E longitude, originating in the Phi Pan Nam Range and flowing 460 km southward to merge with the Ping River near Tak Province, 30 km downstream of the Bhumibol Dam (Bidorn et al., 2015; Charoenlerkthawin et al., 2021). The river gradient varies between 1:60 and 1:4,000 (Bidorn et al., 2015).

The basin's land use is primarily forest (73.09%), followed by agricultural land (18.29%), and urban or built-up areas (3.98%) (Raveephinit et al., 2021). The average annual rainfall is 1,100 mm, with 88% occurring during the wet season (May–October) (Bidorn et al., 2015; Raveephinit et al., 2021). Despite its small size, the Wang River Basin is hydrologically significant, sharing sediment and flow characteristics with the neighboring Ping River Basin. Notably, extreme events like the 2011 flood highlighted its vulnerability to sediment transport and flooding (Bidorn et al., 2015).

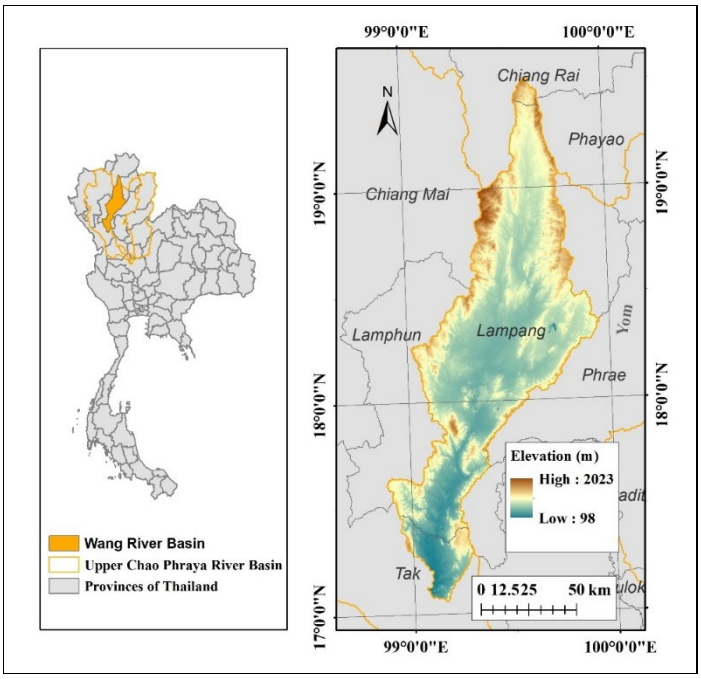

Figure 1 Study area

3. METHODOLOGY

As shown in Figure 2. The methodology involved four main steps: Data Preparation, Flood Conditioning Factors Selection, Flood Susceptibility Mapping, and Model Evaluation.

Data Preparation: The study began by collecting data on 13 flood conditioning factors, including aspect, curvature, distance from river, elevation, geology, land use/land cover (LULC), NDVI, precipitation, river density, slope, soil permeability, SPI, and TWI. These factors were clipped to the Wang River Basin boundary and were preprocessed into uniform raster formats. Flood inventory data, containing 3,000 flood and 3,000 non-flood points, was divided into a training set (70%) for model development and a verification set (30%) for independent evaluation.

Flood Conditioning Factors Selection: A multicollinearity check was performed using Pearson's correlation coefficient to identify and eliminate redundant factors, ensuring that selected factors are statistically independent. Shannon Entropy was then applied to calculate the weight (W_i) of each factor based on its contribution to past flood occurrences. Only factors with $W_i > 0.05$ were retained for further analysis.

Flood Susceptibility Mapping: The selected factors were re-weighted using SE to enhance their contributions. Two modeling approaches were employed to generate flood susceptibility maps: SE modeling and RF modeling.

Model Evaluation: The flood susceptibility maps produced by both models were validated using training and verification datasets. Model performance was assessed based on AUC-ROC (Area Under Curve - Receiver Operating Characteristic) metrics, comparing the effectiveness of SE and RF models in predicting flood-prone areas.

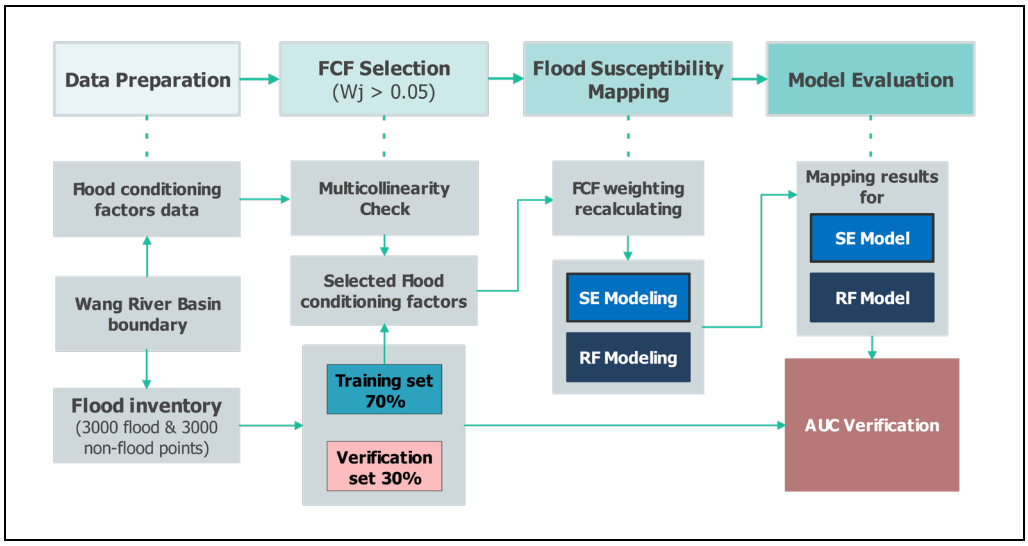

Figure 2 Methodology flowchart

3.1 Data preparation

Flood inventory refers to extensive database of historical floods in a region, including locations, extents, and frequencies. Such inventories are key components of FSM since they offer fundamental observations that enable identifying the flood risk areas which can inform subsequent assessment and mitigation (Wahba et al., 2024). In this study, flood inventory data obtained from Thailand's Geo-Informatics and Space Technology Development Agency (GISTDA) portal (https://disaster.gistda.or.th/flood/repeat) was adopted, which offers historical flood extents from 2006 to 2022. This dataset was adopted in the study of Long et al. (2025) and was verified to be effective in FSM study. A total of 3000 flood and 3000 non-flood points were randomly sampled from this dataset for developing and validating the flood susceptibility models.

FCFs are environmental factors affecting the frequency and magnitude of flooding events. These include natural factors (such as the topography of the land and the amount of rainfall) and anthropogenic factors (such as land use and soil permeability). Since FCFs play an important role in the pre-disaster planning process by determining the areas that are more vulnerable to flooding to generate accurate flood susceptibility maps, FCFs should be well understood and assessed (Kaya & Derin, 2023). The examination of these factors allows researchers to analyze the extent to which variables of climate and human impact contribute to flood hazards and therefore implement strategies for flood risk management.

Thirteen commonly adopted FCFs were initially selected in this study: aspect, curvature, distance from river, elevation, geology, land use/land cover (LULC), NDVI, precipitation, river density, slope, soil permeability, SPI, and topographic wetness index (TWI). These FCFs were then tested and screened. The data sources of these FCFs are listed in Table 1.

Table 1 FCFs data source

Factor(s)	Data Name	Time	Source	Resolution
Elevation, slope, aspect, curvature, TWI, SPI	SRTM DEM	-	United States Geological Survey (USGS) https://earthexplorer.usgs.gov/	30 m raster
LULC	Land use	2021	LDD https://tswc.ldd.go.th/	Vector
Precipitation	Rainfall	1981–2022	Northern Meteorological Center http://www.cmmet.tmd.go.th/	Vector
Soil permeability	Soil group	2018	Land Development Department (LDD) https://tswc.ldd.go.th/	Vector
Distance from river and River density	River	2017	Water Analysis and Assessment Division, Thailand http://mekhala.dwr.go.th/	Vector
Geology	Generalized Geology of Southeast Asia	-	USGS https://certmapper.cr.usgs.gov/data/apps	Vector
NDVI	Landsat 8 OLI/TIRS Level-2 data	2022	USGS https://earthexplorer.usgs.gov/	30 m raster

The thematic layers for the 13 FCFs are shown in Figure 3, which included aspect (a), curvature (b), distance from the river (c), elevation (d), geology (e), LULC (f), NDVI (g), precipitation (h), river density (i), slope (j), soil permeability (k), SPI (l), and TWI (m). The vector and raster datasets, obtained as explained in Table 1, were pre-processed to provide consistency over the study area. All of them were homogenized with a spatial resolution of 30 meters so that it can fit into the scale of modeling.

Aspect refers to the direction a slope faces, influencing sunlight exposure and vegetation growth, which can affect runoff patterns. It can modulate water flow direction and accumulation in certain terrains (Al-Kindi & Alabri, 2024). Curvature describes the shape of the terrain, with concave areas more prone to water accumulation and convex areas facilitating runoff. It is a critical morphological factor in flood modeling (Pham et al., 2021). Proximity to rivers is a primary factor in flood susceptibility, as areas closer to rivers are more likely to experience inundation during high-flow events. This factor is often used to define buffer zones for flood risk assessment (Dey et al., 2024). Elevation is a fundamental factor in flood modeling, as low-lying areas are more prone to flooding due to water accumulation. Higher elevations generally reduce flood risk but can influence downstream flow patterns (Riche et al., 2024). Geological composition affects water infiltration and runoff, with impermeable rocks increasing surface runoff and flood risk. Permeable rocks, such as sandstones, reduce flood susceptibility by allowing water infiltration (Gohil et al., 2024). LULC influences hydrological responses, with urban areas increasing impervious surfaces and runoff, while forests and wetlands promote water infiltration and storage. It is a key factor in FSM (Yu et al., 2023). NDVI measures vegetation density, which affects water retention and runoff. Higher NDVI values indicate denser vegetation, reducing flood risk by enhancing infiltration and slowing surface flow (Rahmati et al., 2020). Precipitation is a direct driver of flooding, with higher rainfall amounts increasing the likelihood of flood events. It is a critical meteorological factor in flood susceptibility modeling (Akay, 2024). River density, defined as the length of drainage lines per unit area, is a key factor in flood susceptibility. Higher river density increases the likelihood of flooding due to greater water concentration (Pham et al., 2021). Slope influences runoff velocity and volume, with steeper slopes leading to faster runoff and increased flood risk downstream. It is a critical topographical factor in flood modeling (Al-Kindi & Alabri, 2024). Soil permeability determines the rate of water infiltration, with low permeability soils increasing surface runoff and flood risk. It is a key hydrological factor in flood susceptibility assessment (Dey et al., 2024). SPI measures the erosive power of flowing water, with higher values indicating greater flood potential. It is a key hydrometric factor in flood susceptibility mapping (Riche et al., 2024). TWI quantifies the tendency of water to accumulate in specific areas based on slope and flow accumulation. It is a critical factor in identifying flood-prone zones (Yu et al., 2023).

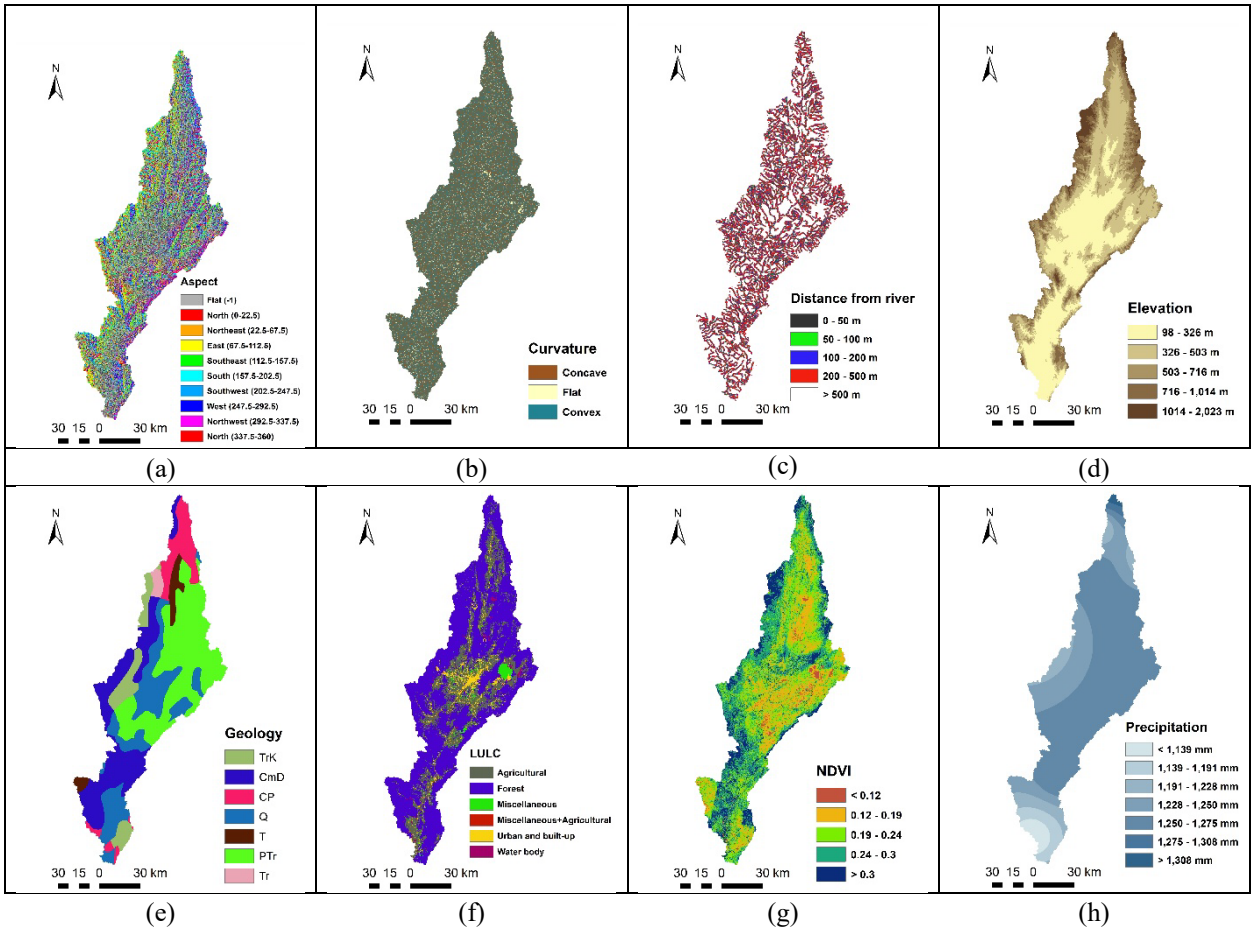

Figure 3 The FCF thematic layers for aspect (a), curvature (b), distance from river (c), elevation (d), geology (e), LULC (f), NDVI (g), precipitation (h), river density (i), slope (j), soil permeability (k), SPI (l), and TWI (m)

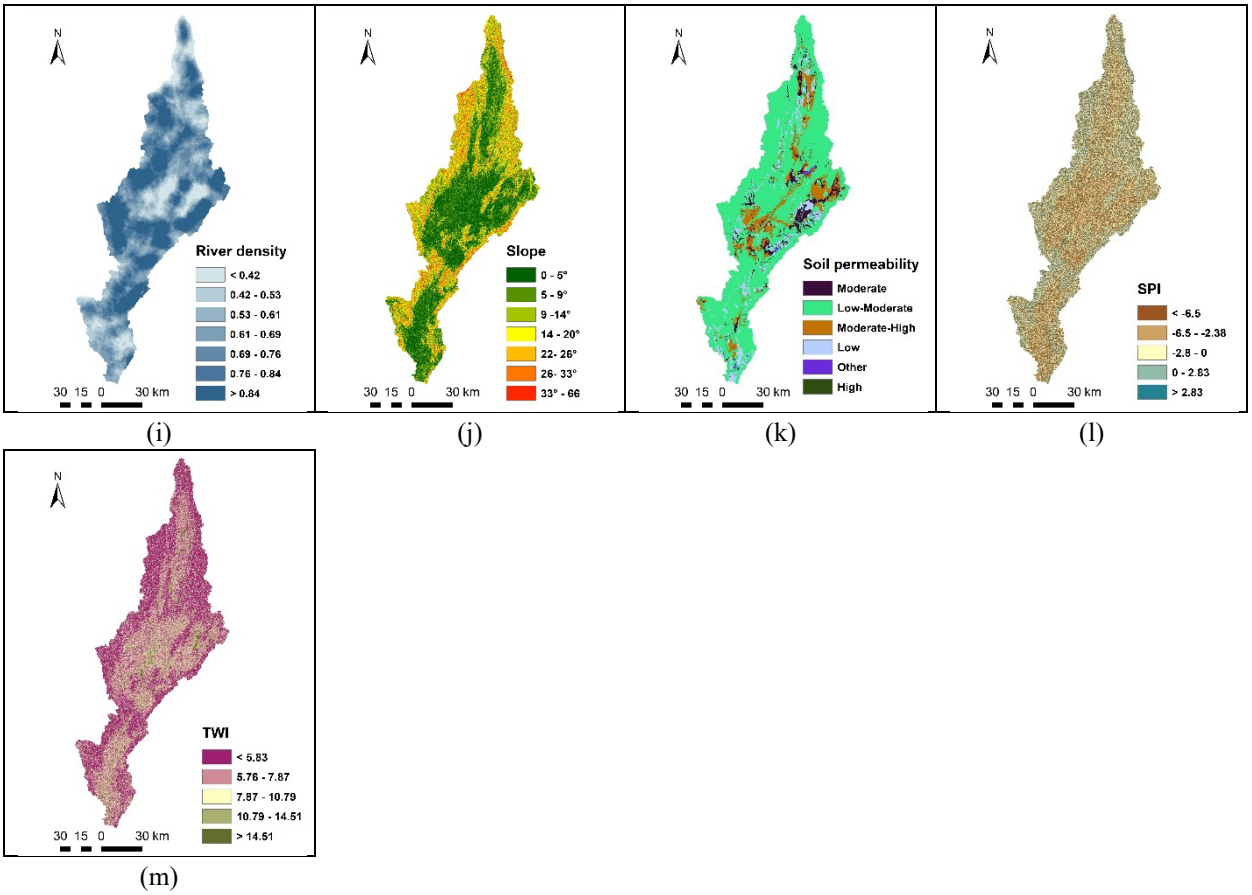

Figure 3 The FCF thematic layers for aspect (a), curvature (b), distance from river (c), elevation (d), geology (e), LULC (f), NDVI (g), precipitation (h), river density (i), slope (j), soil permeability (k), SPI (l), and TWI (m) (continued)

3.2 Shannon's Entropy

SE is a key information theoretical concept, first introduced by Claude Shannon in 1948 (Rahaman et al., 2021), which measures the level of uncertainty or disorder in a system. Specifically, SE is used in FSM to evaluate the relative contribution of factors which contribute to floods, thus helping in determining the prone areas. The SE model enhances traditional methods by quantifying system instability and uncertainties, allowing for the determination of the most influential factors in flood susceptibility (Haghizadeh et al., 2017).

The SE index, which links quantity with entropy, is particularly useful for modeling flood susceptibility and can be calculated using the following equations.

The Frequency Ratio (FR_{ij}) is calculated as:

$$FR_{ij} = \frac{N_{ij}^{f} / N^{f}}{N_{ij} / N} \tag{1}$$

where i and j denotes the FCF number and class number, N_{ij}^{f} represents the number of pixels in each FCF class, N^{f} denotes the total number of pixels in the study area, N_{ij} is the number of flood pixels in each FCF class, N is the total number of all flooded pixels in the study area.

The probability density P_{ij} for each class is calculated as:

$$P_{ij} = \frac{FR_{ij}}{\sum_{j=1}^{i} FR_{ij}}, i = 1, \ldots, m \tag{2}$$

where P_{ij} probability density of each class; followed by:

$$K_i = -\frac{1}{\ln(n_i)} \tag{3}$$

$$E_i = K_i \sum_{j=1}^{i} P_{ij} \ln(P_{ij}) \tag{4}$$

$$D_i = 1 - E_i \tag{5}$$

$$W_i = \frac{D_i}{\sum_{i=1}^{m} D_i}, \; i = 1, \ldots, m \tag{6}$$

where K_i is the computed coefficient for FCF i, n_i is the number of classes of FCF i, and m refers to the number of FCFs. E_i denotes the Entropy of FCF i, D_i is the degree of divergence for FCF i. W_i is the weighting value of FCF i, of which range obtained is between 0 and 1. A value closer to 1 indicates higher inconsistency and imbalance.

To conduct FSM for the area using the SE method, the flood susceptibility index (FSI) must be defined; it is calculated using Eq. (8):

$$C_{ij} = P_{ij} \times 100 \quad (7)$$

$$FSI = \sum \left(W_i C_{ij} \right) \quad (8)$$

where C_{ij} is the weighting value for each class. A high FSI value implies a higher probability of flood occurrence, whereas a low FSI value indicates a lower likelihood of flood occurrence.

3.3 Flood Conditioning Factors Selection

Multicollinearity check

In this study, multicollinearity among the 13 FCFs was assessed using Pearson's correlation coefficient. A commonly accepted threshold for identifying significant collinearity is a Pearson's correlation coefficient greater than 0.7 (Tehrany et al., 2019). The correlation heatmap (Figure 4) visually represented these relationships, with each cell displaying the Pearson's correlation coefficient between a pair of FCFs. In this work, the highest correlation observed was between slope and elevation, with a coefficient of 0.57. This value is below the 0.7 threshold, indicating that multicollinearity among the FCFs was not a concern in this study.

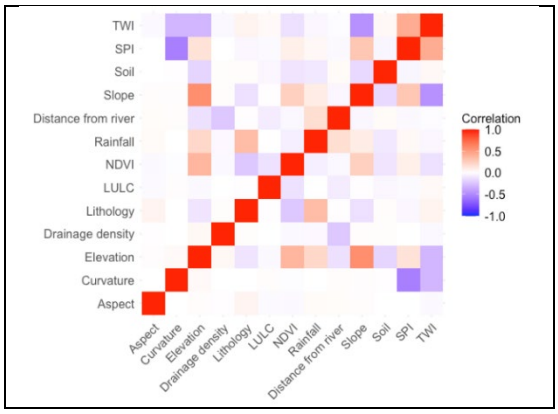

Figure 4. Correlation heatmap of the FCFs

FCFs selection and weighting using SE

Figure 5 presents the calculated weight values (W_i) for the 13 FCFs. Among these, certain factors such as aspect, curvature, and distance from river exhibited weight values close to or approximately 0, indicating minimal contributions to flood susceptibility. Other factors, while exhibiting higher weights, remained below the threshold of 0.5. Factors with negligible or very low W_i values were marked in red in Figure 4 to highlight their limited relevance. Based on this analysis, only seven key FCFs were retained for further modeling: curvature (0.21), slope (0.14), elevation (0.19), geology (0.16), soil permeability (0.12), precipitation (0.09), and SPI (0.06).

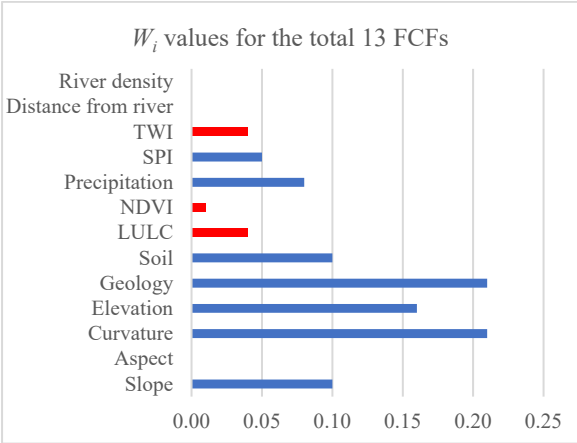

Figure 5 W_i values for the 13 FCFs

Table 2 summarizes the selected FCFs, their classification details, and respective weighting values. The table includes essential metrics for each FCF, such as class, area of each class in square kilometers and percentage to total area, number and percentage of flood points in each class, the Frequency Ratio (FR_{ij}), probability density (P_{ij}), and class weighting (C_{ij}).

The W_i values represent the recalculated importance weights for the seven selected FCFs, highlighting their significance in flood susceptibility modeling. These weights represent the overall contribution of factors to flood spatial distribution, which are based on the relationship of each factor to past flood events. C_{ij}values, on the other hand, quantify the contribution of the classes in each FCF, representing their relative effect on flood occurrence. Collectively, these weights provide a strategic framework for understanding and prioritizing FCFs in the flood susceptibility analysis.

Table 2 Selected FCFs and their classification details, and their respective weighing values

Factor	Class	Area (km²)	Area %	Flood points	Flood points %	FR_{ij}	P_{ij}	C_{ij}	W_j
Slope	0 - 5°	3183.66	29.87%	1450	69.00%	2.31	0.60	60	0.11
	5 - 9	2372.97	22.26%	539	26.00%	1.15	0.30	30	
	9 -14°	1684.63	15.80%	85	4.00%	0.26	0.07	7	
	14 - 20°	1471.53	13.81%	18	1.00%	0.06	0.02	2	
	22- 26°	1066.91	10.01%	8	0.00%	0.04	0.01	1	
	26- 33°	644.87	6.05%	1	0.00%	0.01	0.00	0	
	33 - 66°	234.50	2.20%	0	0.00%	0.00	0.00	0	
Curvature	Concave	5102.20	47.87%	1004	48.00%	1.00	0.32	32	0.23
	Flat	584.53	5.48%	136	6.00%	1.18	0.37	37	
	Convex	4972.34	46.65%	961	46.00%	0.98	0.31	31	
Elevation	98 - 326 m	3889.76	36.49%	1950	93.00%	2.54	0.92	92	0.18
	326 - 503 m	3293.09	30.89%	150	7.00%	0.23	0.08	8	
	503 - 716 m	1926.30	18.07%	1	0.00%	0.00	0.00	0	
	716 - 1,014 m	1200.61	11.26%	0	0.00%	0.00	0.00	0	
	1014 - 2,023 m	349.32	3.28%	0	0.00%	0.00	0.00	0	
Geology	Triassic-Cretaceous	853.30	8.01%	70	3.00%	0.42	0.07	7	0.23
	Cambrian Dolomite	2398.53	22.50%	226	11.00%	0.48	0.08	8	
	Carboniferous-Permian	974.21	9.14%	132	6.00%	0.69	0.12	12	
	Quaternary	2316.11	21.73%	1133	54.00%	2.48	0.43	43	
	Tertiary	360.24	3.38%	76	4.00%	1.07	0.18	18	
	Permian-Triassic	3607.00	33.84%	464	22.00%	0.65	0.11	11	
	Triassic	149.68	1.40%	0	0.00%	0.00	0.00	0	
Precipitation	< 1,139 m	291.24	2.73%	282	13.00%	4.91	0.62	62	0.09
	1,139 - 1,191 m	479.02	4.49%	92	4.00%	0.97	0.12	12	
	1,191 - 1,228 m	806.94	7.57%	35	2.00%	0.22	0.03	3	
	1,228 - 1,250 m	2279.22	21.38%	375	18.00%	0.83	0.11	11	
	1,250 - 1,275 m	6686.93	62.73%	1317	63.00%	1.00	0.13	13	
	1,275 - 1,308 m	66.62	0.63%	0	0.00%	0.00	0.00	0	
	> 1,478 m	49.09	0.46%	0	0.00%	0.00	0.00	0	
Soil	Moderate	645.59	6.06%	153	7.00%	1.20	0.07	7	0.11
	Low-Moderate	8019.18	75.23%	1411	67.00%	0.89	0.05	5	
	Moderate-High	1151.06	10.80%	477	23.00%	2.10	0.12	12	
	Low	800.61	7.51%	52	2.00%	0.33	0.02	2	
	Other	39.05	0.37%	0	0.00%	0.00	0.00	0	
	High	3.20	0.03%	8	0.00%	12.70	0.74	74	
SPI	< -6.5	4094.50	38.41%	718	34.00%	0.89	0.13	13	0.05
	-6.5 - -2.38	864.72	8.11%	679	32.00%	3.98	0.56	56	
	-2.8 - 0	3064.52	28.75%	451	21.00%	0.75	0.11	11	
	0 - 2.83	2141.07	20.09%	146	7.00%	0.35	0.05	5	
	> 2.83	494.27	4.64%	107	5.00%	1.10	0.16	16	

3.4 Random Forest

RF is an ensemble-based machine learning algorithm which creates decision trees based on random data and feature samples and then aggregates the output to improve accuracy and reduce overfitting. In flood susceptibility mapping (FSM), RF is extremely useful to rank complex, high-dimensional environmental data in FSM (Dey et al., 2024; Seydi et al., 2022)—such as topography, precipitation, and land use—by effectively ranking the importance of these factors. RF model was built in R using the caret package. Hyperparameters were tuned via 10-fold cross-validation optimizing for AUC ("ROC"). and the number of trees was set to 1,000 (ntree = 1000). The best mtry (by highest ROC) was selected for the final RF model.

4. Results and Discussion

4.1 AUC evaluation results

ROC curves of SE and RF models on training and verification datasets were shown in Figure 6. The ROC curves provided visualization of models' classification accuracy; the curves closer to the top-left corner indicate higher sensitivity and specificity.

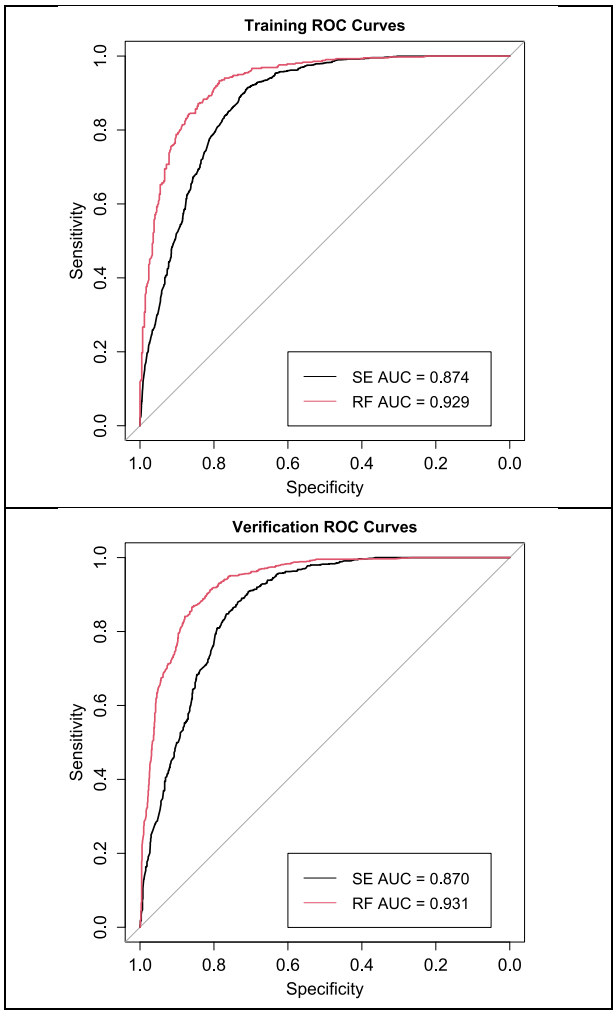

Figure 6 ROC curves of SE and RF models based on both training and verification dataset

In general, the performance of both two models was satisfactory, obtaining AUC higher than 0.870 in both two train and verification datasets. The SE model performed reasonably well with an AUC of 0.874 (training) and 0.870 (verification) but was outperformed by the RF model which achieved an AUC of 0.929 (training) and 0.931 (verification).

We observed the trade-off of generalizability between training and verification results. An important note was that the AUC values show consistency of training and verification datasets for both models, neither of which reflected overfitting but provided robust performance. This demonstrated that the models were both accurate with new data. In FSM, creating practical models that can be expected to make accurate predictions in the real world is the main objective; thus, this balance is critical. Both models showed relatively high AUC values confirming the appropriateness of the FCFs selection and preprocessing for the study area. Particularly, the SE feature selection and the combination with RF was remarkable in terms of predictive robustness and reliability.

Most notably, the RF model in our study significantly outperformed the SE model, reinforcing the superior predictive power of the state of art ML methods introduced. This finding was consistent with previous studies that ML models consistently perform better than traditional statistical methods. For example, Seydi et al. (2022) and Bhattarai et al. (2024) have both reported that single ML models lead to more FSM accuracy and robustness than traditional statistical approaches. The superior performance of RF was likely due to its ability to capture non-linear interactions among multiple flood conditioning factors, which SE—being based on independent weighting—could not fully exploit. RF's ensemble of decision trees allowed it to model complex, high-dimensional relationships and automatically prioritize the most informative predictors, thereby enhancing discrimination between flood and non-flood points.

4.2 Flood susceptibility results

Figure 7 presents the flood susceptibility maps produced using the SE and RF models, categorizing the study area into five susceptibility levels: Very Low, Low, Moderate, High, and Very High. These maps represented the spatial variation of flood-prone areas across the study region, with noticeable differences in the distribution and extent of susceptibility levels.

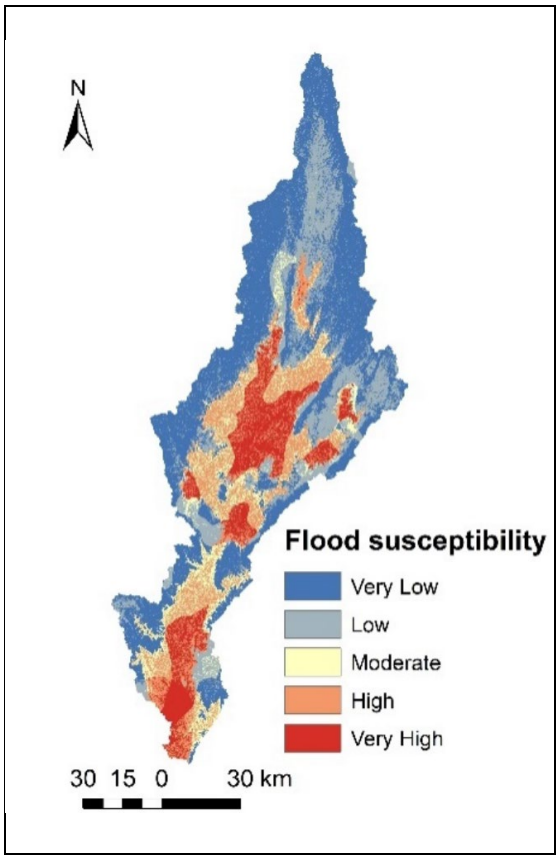

(a)

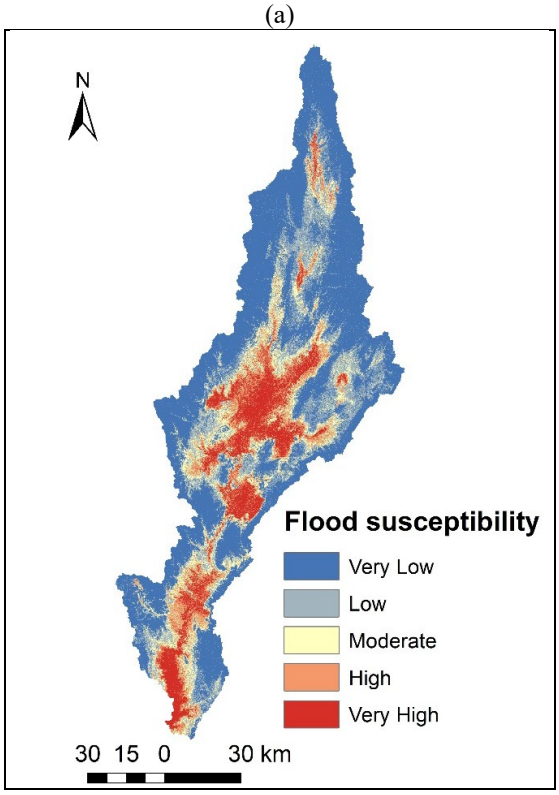

(b)

Figure 7 Floods susceptibility mapping results for SE (a) and RF (b) models

Figure 8 highlights the percentages and total areas of different flood susceptibility levels for the SE and RF models. The SE model predicted 41.58% of the area as "Very Low" susceptibility, while the RF model increased this proportion to 51.09%, suggesting that RF was more conservative in predicting higher susceptibility levels. On the contrary, SE identified larger proportions of "High" (16.64%) and "Very High" (11.20%) susceptibility areas compared to RF (9.87% and 10.62%, respectively). When examining the total area (in square kilometers) under each susceptibility level, the SE model classified 4432.07 km² as "Very Low," 2182.81 km² as "Low," 1076.52 km² as "Moderate," 1773.63 km² as "High," and 1193.66 km² as "Very High." Meanwhile, the RF model classified 5445.74 km² as "Very Low," 1775.14 km² as "Low," 1253.75 km² as "Moderate," 1051.92 km² as "High," and 1132.15 km² as "Very High." These results suggested that the RF model exhibited a tendency to assign a greater portion of the study area to "Very Low" and "Moderate" susceptibility levels, potentially underestimating higher susceptibility zones. Conversely, the SE model appeared to provide a more balanced and inclusive representation of flood susceptibility, identifying a larger area as "High" and "Very High" susceptibility.

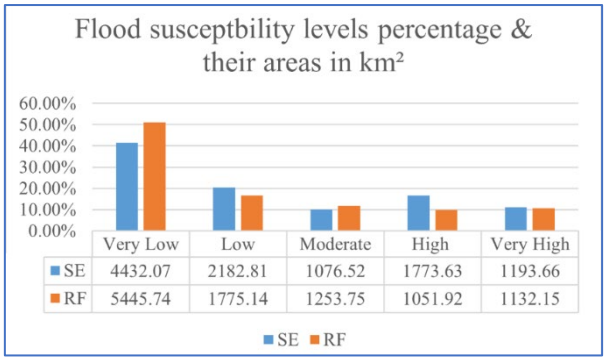

Figure 8 Floods susceptibility levels percentage and the areas for SE and RF models

The differences between the models may stem from their underlying methodologies. The SE model integrated multiple factors systematically, leading to a broader spread across all susceptibility levels. In contrast, the RF model's decision tree-based mechanism emphasized dominant factors, which could explain its conservative predictions for high-susceptibility areas.

The results emphasized the advantages of ML models in FSM. Their ability to delineate high-risk areas with greater accuracy can significantly enhance flood mitigation planning and risk management efforts. The variation in susceptibility distributions across models highlighted the importance of algorithm selection based on specific modeling objectives and the characteristics of the study area.

5. Conclusion

This study demonstrated that modern ML techniques significantly outperformed conventional statistical approaches—such as the Shannon Entropy method—in mapping flood susceptibility within Thailand's Wang River Basin. By integrating a comprehensive set of 13 flood conditioning factors (including aspect, curvature, elevation, geology, LULC, NDVI, precipitation, river density, slope, soil permeability, SPI, and TWI) with a robust flood inventory of 3000 flood and 3000 non-flood samples, we were able to build a well-balanced and informative dataset. Multicollinearity among the factors was carefully assessed using the Pearson correlation method, ensuring that the predictive models were not adversely affected by redundant information. The SE method was used to identify the contribution of each FCF to the occurrence of floods, by setting the importance weight threshold W_i, FCFs with $W_i > 0.5$ including curvature, slope, elevation, geology, soil permeability, precipitation, and SPI were kept into the modeling process.

The performance of SE versus RF models was investigated in this study. The results consistently showed that the RF obtained higher AUC both on training and verification datasets than the SE model, indicating that advanced ML methods are suitable to manage the dynamic and heterogeneous nature of flood susceptibility, resulting in improvement of prediction accuracy and operational stability at Wang River Basin. In addition, the flood susceptibility maps produced in this study provide useful information that helps with flood management and risk reduction by identifying and quantifying areas with a high risk of flooding that should be targeted for interventions by local authorities. Despite these promising outcomes, challenges remain—particularly regarding model interpretability, data quality, and the need for improved generalization across diverse regions. Future studies could explore more elaborate hybrid schemes (i.e., physics-based deep learning and probabilistic), for further enhancing predictive power while ensuring that model outputs are both transparent and actionable for decision-makers.

Overall, this study highlighted the transformative potential of ML in FSM and underscored its critical role in developing rapid, accurate, and scalable flood forecasting systems to mitigate the adverse impacts of extreme weather events in the Wang River Basin and beyond.

6. Acknowledgments

This work was supported and funded by Naresuan University Faculty of Engineering Scholarships.

7. References

Akay, H. (2024). Flood Susceptibility Mapping Using Information Fusion Paradigm Integrated with Decision Trees. *Water Resources Management*, *38*(13), 5365-5383. https://doi.org/10.1007/s11269-024-03918-5

Al-Kindi, K. M., & Alabri, Z. (2024). Investigating the Role of the Key Conditioning Factors in Flood Susceptibility Mapping Through Machine Learning Approaches. *Earth Systems and Environment*, *8*(1), 63-81. https://doi.org/10.1007/s41748-023-00369-7

Bhattarai, Y., Duwal, S., Sharma, S., & Talchabhadel, R. (2024). Leveraging machine learning and open-source spatial datasets to enhance flood susceptibility mapping in transboundary river basin. *International Journal of Digital Earth*, *17*(1). https://doi.org/10.1080/17538947.2024.2313857

Bidorn, B., Chanyotha, S., Kish, S. A., Donoghue, J. F., Bidorn, K., & Mama, R. (2015). The effects of Thailand's Great Flood of 2011 on river sediment discharge in the upper Chao Phraya River basin, Thailand. *International Journal of Sediment Research*, *30*(4), 328-337. https://doi.org/10.1016/j.ijsrc.2015.10.001

Charoenlerkthawin, W., Namsai, M., Bidorn, K., Rukvichai, C., Panneerselvam, B., & Bidorn, B. (2021). Effects of Dam Construction in the Wang River on Sediment Regimes in the Chao Phraya River Basin. *Water*, *13*(16). https://doi.org/10.3390/w13162146

Dey, H., Shao, W., Moradkhani, H., Keim, B. D., & Peter, B. G. (2024). Urban flood susceptibility mapping using frequency ratio and multiple decision tree-based machine learning models. *Natural Hazards*, *120*(11), 10365-10393. https://doi.org/10.1007/s11069-024-06609-x

Gohil, M., Mehta, D., & Shaikh, M. (2024). An integration of geospatial and fuzzy-logic techniques for flood-hazard mapping. *Journal of Earth System Science*, *133*(2). https://doi.org/10.1007/s12040-024-02288-1

Haghizadeh, A., Siahkamari, S., Haghiabi, A. H., & Rahmati, O. (2017). Forecasting flood-prone areas using Shannon's entropy model. *Journal of Earth System Science*, *126*(3). https://doi.org/10.1007/s12040-017-0819-x

Kaya, C. M., & Derin, L. (2023). Parameters and methods used in flood susceptibility mapping: a review. *Journal of Water and Climate Change*, *14*(6), 1935-1960. https://doi.org/10.2166/wcc.2023.035

Long, G., Tantanee, S., Nusit, K., & Sooraksa, P. (2025). Flood susceptibility mapping in the Yom River Basin, Thailand: stacking ensemble learning using multi-year flood inventory data. *Geocarto International*, *40*(1). https://doi.org/10.1080/10106049.2025.2461531

Pham, B. T., Jaafari, A., Phong, T. V., Yen, H. P. H., Tuyen, T. T., Luong, V. V., Nguyen, H. D., Le, H. V., & Foong, L. K. (2021). Improved flood susceptibility mapping using a best first decision tree integrated with ensemble learning techniques. *Geoscience Frontiers*, *12*(3). https://doi.org/10.1016/j.gsf.2020.11.003

Rahaman, A., Venkatesan, M. S., & Ayyamperumal, R. (2021). GIS-based landslide susceptibility mapping method and Shannon entropy model: a case study on Sakaleshapur Taluk, Western Ghats, Karnataka, India. *Arabian Journal of Geosciences*, *14*(20). https://doi.org/10.1007/s12517-021-08422-3

Rahmati, O., Darabi, H., Panahi, M., Kalantari, Z., Naghibi, S. A., Ferreira, C. S. S., Kornejady, A., Karimidastenaei, Z., Mohammadi, F., Stefanidis, S., Tien Bui, D., & Haghighi, A. T. (2020). Development of novel

hybridized models for urban flood susceptibility mapping. *Sci Rep*, *10*(1), 12937. https://doi.org/10.1038/s41598-020-69703-7

Raveephinit, D., Rittima, A., Phankamolsil, Y., Tabucanon, A. S., Sawangphol, W., Kraisangka, J., Talaluxmana, Y., & Vudhivanich, a. V. (2021). *Assessment of Weap Model in Simulating Rainfall-Runoff Relation in The Ping and Wang River Basins, Thailand* The 8th National Conference on Water Resources Engineering & The 5th International Conference on Water Resources Engineering, Department of irrigation engineering, Faculty of engineering at kamphaeng saen, Kasetsart University.

Riche, A., Drias, A., Guermoui, M., Gherib, T., Boulmaiz, T., Souissi, B., & Melgani, F. (2024). A Novel Hybrid Deep-Learning Approach for Flood-Susceptibility Mapping. *Remote Sensing*, *16*(19). https://doi.org/10.3390/rs16193673

Seydi, S. T., Kanani-Sadat, Y., Hasanlou, M., Sahraei, R., Chanussot, J., & Amani, M. (2022). Comparison of Machine Learning Algorithms for Flood Susceptibility Mapping. *Remote Sensing*, *15*(1). https://doi.org/10.3390/rs15010192

Tehrany, M. S., Jones, S., & Shabani, F. (2019). Identifying the essential flood conditioning factors for flood prone area mapping using machine learning techniques. *Catena*, *175*, 174-192. https://doi.org/10.1016/j.catena.2018.12.011

Wahba, M., Sharaan, M., Elsadek, W. M., Kanae, S., & Hassan, H. S. (2024). Examination of the efficacy of machine learning approaches in the generation of flood susceptibility maps. *Environmental Earth Sciences*, *83*(14). https://doi.org/10.1007/s12665-024-11696-x

Yu, H., Luo, Z., Wang, L., Ding, X., & Wang, S. (2023). Improving the Accuracy of Flood Susceptibility Prediction by Combining Machine Learning Models and the Expanded Flood Inventory Data. *Remote Sensing*, *15*(14). https://doi.org/10.3390/rs15143601